

Digital Solid-State SPECT/CT Quantitation of Absolute ^{177}Lu Radiotracer Concentration: In Vivo and In Vitro Validation

John A. Kennedy^{1,2}, Rachel Lugassi¹, Ronit Gill¹, and Zohar Keidar^{1,2}

¹Department of Nuclear Medicine, Rambam Health Care Campus, Haifa, Israel; and ²Ruth and Bruce Rappaport Faculty of Medicine, Technion-Israel Institute of Technology, Haifa, Israel

The accuracy of ^{177}Lu radiotracer concentration measurements using quantitative clinical software was determined by comparing in vivo results for a digital solid-state cadmium-zinc-telluride SPECT/CT system with in vitro sampling. **Methods:** First, image acquisition parameters were assessed for an International Electrotechnical Commission body phantom emulating clinical count rates loaded with a lung insert and 6 hot spheres with a 12:1 target-to-background ratio of ^{177}Lu solution. Then, the data of 28 whole-body SPECT/CT scans of 7 patients who underwent ^{177}Lu prostate-specific membrane antigen radioligand therapy were retrospectively analyzed. Three users analyzed SPECT/CT images for in vivo urinary bladder radiotracer uptake using quantitative software. In vitro radiopharmaceutical concentrations were calculated using urine sampling obtained immediately after each scan, scaled to SUVs. Any in vivo or in vitro identity relations were determined by linear regression (ideally, slope = 1 and intercept = 0), within a 95% confidence interval. **Results:** Phantom results demonstrated lower quantitative error for acquisitions using the 113-keV ^{177}Lu energy peak rather than including the 208-keV peak, given that only low-energy collimation was available in this camera configuration. In the clinical study, 24 in vivo-in vitro pairs were eligible for further analysis, with 4 having been rejected as outliers (via Cook distance calculations). All linear regressions ($R^2 \geq 0.82$, $P < 0.0001$) provided identity in vivo-in vitro relations (95% confidence interval), with SUV averages from all users giving a slope of 0.96 ± 0.13 , an intercept of $-0.07 \pm 0.46 \text{ g/mL}$, and an average residual difference of 19.5%. In acquisitions with the lower-energy ^{177}Lu energy peak, solid-state SPECT/CT imaging provided an accuracy to within approximately 20% of in vivo urinary bladder radiotracer concentrations. **Conclusion:** This noninvasive in vivo quantitation method can potentially improve diagnosis, patient management, and treatment response assessment and provide data essential to ^{177}Lu dosimetry.

Key Words: SPECT/CT; quantitation; PSMA; Lu-177; CZT

J Nucl Med 2020; 61:1381–1387

DOI: 10.2967/jnumed.119.239277

Prostate-specific membrane antigen (PSMA) radiolabeled with ^{177}Lu is a novel therapeutic option for patients with advanced metastatic castration-resistant prostate cancer. Given resistance or contraindications to conventional therapies, and proven PSMA-expressing

tumors via imaging (e.g., ^{68}Ga -PSMA PET), ^{177}Lu -PSMA shows promise (1). This $^{177}\text{Lu}/^{68}\text{Ga}$ radiopharmaceutical pair is one of a broader range of treatment–diagnostic pairs in the relatively new branch of theranostics in nuclear medicine (2). A typical treatment consists of up to 6 or 7 cycles of an activity of 6 to 7.4 GBq of ^{177}Lu -PSMA at intervals of 6–8 wk (3). The concept is that PSMA-expressing cancer cells preferentially incorporate the PSMA ligand along with the ^{177}Lu label. β -radiation (0.498-MeV maximum energy) is emitted as part of the ^{177}Lu decay, which has a half-life of 159.6 h (3). Auger and conversion electrons also contribute significantly to the spectrum of high-energy electrons emitted (4). This radiation is cytotoxic and may cause tumor necrosis.

SPECT/CT imaging provides a means to visually assess the body distribution of the treatment dose and to evaluate the response to therapy by demonstrating ^{177}Lu -PSMA uptake in prostate cancer lesions. Quantitative SPECT imaging enables a nonsubjective tracking of response to treatment by providing absolute measures of ^{177}Lu -PSMA uptake in the tumor. Additionally, quantitative SPECT provides data essential for dosimetry of ^{177}Lu -PSMA (5) as well as of other ^{177}Lu -radiolabeled ligands (6–8) and other radiotherapies currently of interest in the medical community (1,7,9). In general, there has been interest in absolute quantitative SPECT since the common implementation of the modality (10–12), further enabled by the advent of SPECT/CT hybrid systems, which provide a registered CT scan useful for attenuation correction of absorbed γ -ray photons (13,14). SPECT/CT also provides added clinical value by the precise localization of radiotracer uptake (15–17). Quantitative SPECT/CT has the potential to improve clinical outcomes, with direct applications in additional areas such as assessing disease progression, measuring coronary flow reserve, and performing neurotransmitter brain imaging of receptor density and occupancy (10).

Currently, the available computing power for commercial SPECT/CT systems has led to the clinical use of iterative reconstruction algorithms that can correct for the effects of collimation (collimator modeling or resolution recovery), scatter, and attenuation, ameliorating artifactual results that degrade absolute quantitative results. Additionally, current imaging workstations can be provided with commercial quantitative software that facilitates the tasks necessary for practical quantitation, such as tools for drawing volumes of interest (VOIs) and calculating decay-corrected radiopharmaceutical concentrations from coregistered SPECT/CT images (18).

In addition to β -emission essential for treatment, ^{177}Lu emits 2 types of γ -rays at energies suitable for SPECT imaging: 113 keV and 208 keV (Table 1). The intensity of these emissions are 6.2% and 10.4% of the decays, respectively (4). These photon count densities are suitable for imaging because they are of the same order of magnitude as diagnostic radiotracers even though the injected activity for treatments is much higher. Appropriate imaging parameters

Received Nov. 7, 2019; revision accepted Jan. 10, 2020.

For correspondence or reprints contact: John A. Kennedy, Department of Nuclear Medicine, Rambam Health Care Campus, P.O. Box 9602, Haifa, Israel, 3109601.

E-mail: j_kennedy@rambam.health.gov.il

Published online Feb. 28, 2020.

COPYRIGHT © 2020 by the Society of Nuclear Medicine and Molecular Imaging.

TABLE 1

Energies and Intensities of γ -Ray Emissions per Nuclear Decay of ^{177}Lu

Energy (keV)	Intensity (%)
71.6	0.172
112.9	6.17
136.7	0.0469
208.4	10.36
249.7	0.2008
321.3	0.210

for quantitative ^{177}Lu SPECT have been investigated previously for conventional sodium iodide Anger cameras (4,19,20). However, a new generation of solid-state-based digital SPECT cameras is now available, using no scintillation or photomultipliers for γ -ray detection. These cameras have cadmium-zinc-telluride (CZT) detectors that provide direct energy conversion in detection (18). These CZT whole-body SPECT systems have the potential to provide better spatial resolution, better energy resolution, and superior patient positioning options (21). The current study aimed to assess the accuracy of ^{177}Lu radiotracer concentration measurements by comparing in vivo results with in vitro sampling using quantitative clinical software and a digital solid-state CZT SPECT/CT system.

MATERIALS AND METHODS

Phantom Study

Image acquisition parameters were assessed for an International Electrotechnical Commission body phantom emulating clinical count rates loaded with a lung insert and 6 hot spheres with a 12.1:1 target-to-background ratio of ^{177}Lu -PSMA in solution. The target-to-background ratio was higher than the 4:1 or 8:1 ratios typically used with this phantom for PET studies (22), and it was chosen both to increase the likelihood that the smallest hot sphere would be imaged and to mimic the comparatively intense ^{177}Lu -PSMA uptake found in prostate cancer patients. The background concentration was 110 kBq/mL at the time of the first acquisition, which was chosen to approximate a clinical count density. Subsequent acquisitions at background concentrations of 65, 29, and 15 kBq/mL were achieved via radiotracer decay. SPECT acquisitions were performed on a digital solid-state whole-body camera (Discovery 670 CZT; GE Healthcare) (18). The camera is hybrid, with a coaxial 16-slice CT gantry. SPECT acquisitions comprised 120 frames, with 3° between frames for a duration of 30 s/frame, on a 128 × 128 matrix. Immediately subsequent CT imaging provided a 2.5-mm slice thickness with a 512 × 512 matrix spanning a 50-cm transverse field of view, acquired using a peak voltage of 120 kV and current ranging from 80 to 200 mA (varied automatically as per object attenuation at each axial location). SPECT reconstruction on a Xeleris Workstation (version 4.0; GE Healthcare) used an ordered-subset expectation maximization algorithm with 10 subsets, 4 iterations, and no postprocessing filter, rendering 4.4-mm voxels. Resolution recovery (collimator modeling), scatter correction, and CT-based attenuation correction were applied within the ordered-subset expectation maximization. The camera configuration used lead collimators with square holes at a pitch of 2.46 mm and a hole length of 5 mm. The septal thickness of 0.2 mm is similar to what is traditionally referred to as low-energy collimation.

For this phantom study, 4 methods were used (Table 2) to compare the effect acquisition parameters. Configured in low-energy mode, only the low-energy ^{177}Lu peak (113 keV) was imaged, since the upper energy peak (208 keV) was truncated. In high-energy mode, the upper

TABLE 2

Phantom Imaging Acquisition Parameters for 4 Methods

Method	Image energy window (keV)		Scatter energy window (keV)	
	Peak(s)	Range	Peak(s)	Range
LE 113 TEW	113	101.7–124.3	96.6	91.6–101.6
			129.4	124.4–134.4
HE 113, 208 TEW	113	101.7–124.3	96.6	91.6–101.6
	208	187.2–228.8	129.4	124.4–134.4
			182	177.5–186.6
			234	229.3–238.7
HE 208 TEW	208	187.2–228.8	182	177.5–186.6
			234	229.3–238.7
HE 208 DEW	208	187.2–228.8	166	145.3–186.7

LE and HE = low and high energy, respectively; 113 and 208 = 113 and 208 keV, respectively; TEW and DEW = triple- and dual-energy windows, respectively.

energy peak could be included either with or without the lower energy peak. The 2 energy modes switch the internal settings of each CZT module, supplying 2 ranges: 50 keV–200 keV and 90 keV–1 MeV. The high-energy resolution may be slightly worse than the low-energy mode.

Generally, triple-energy-window scatter correction was used, except for 1 high-energy, 208-keV peak acquisition using dual-energy-window scatter correction, which was included because it has been shown to give reasonable quantitative results with ^{177}Lu (19). The energy windows used were similar to those found appropriate for quantitative imaging of ^{177}Lu (19). Planar sensitivity (i.e., counts per second per megabecquerel or $\text{s}^{-1} \text{MBq}^{-1}$) for each method was determined for comparison (23). For the phantom, these sensitivities were adjusted as inputs to the commercial quantitative software (described below) in order to give the known volumetric background radiotracer concentration (the ~110 kBq/mL composition) at acquisitions times. Adjusting these volumetric sensitivities is equivalent to adjusting the SPECT calibration factor (24). Each of the 4 acquisition methods required its own volumetric sensitivity value.

Background error and lung residual error were analyzed by methods standard for this phantom (25). Recovery coefficients (ratio of measured to expected radiotracer concentrations) for the 6 hot spheres were based on SUV_{peak} (26). Here, $\text{SUV} = C/[A/m]$, where C is the measured concentration (Bq/mL) from quantitative imaging, A is the decay-corrected activity (Bq), and m is the mass (g) of the phantom background or, in a clinical study, of the patient. By sampling the SUV_{mean} of a 1-mL sphere moved through the VOI, and taking the maximum value, the SUV_{peak} was found. Measurements were made automatically by in-house software after manual slice selection. Recovery coefficients of the 4 different methods were compared by calculating the mean squared error (MSE) from the ideal ratio (12.1:1):

$$\text{MSE} = \frac{1}{6} \sum_{i=1}^6 ((\text{SUV}_{\text{peak}})_i / 12.1 - 1)^2. \quad \text{Eq. 1}$$

Here, the background is expected to have an SUV of 1 g/mL, and the 6 hot spheres (index i) are expected to have SUVs of 12.1, given the 12.1:1 target-to-background ratio. The background error, lung residual

error, and mean squared error of the 4 different phantom acquisition methods for 4 different background concentrations each were compared (t test, $P < 0.05$).

Clinical In Vivo–In Vitro Study

The accuracy of ^{177}Lu radiotracer concentration measurements using quantitative software was determined by comparing clinical in vivo SPECT/CT results with in vitro urine sampling. This method of validation was first described by Zeintl et al. with respect to $^{99\text{m}}\text{Tc}$ quantitation (27). The existing standard practice at our institution comprised whole-body SPECT/CT acquisitions at nominal times of 4, 24, and either 48 or 72 h after ^{177}Lu -PSMA treatment, with a nominal 6-GBq activity (1) and a routine request for a urine sample immediately after imaging. The pelvis was in the field of view of the final bed position to minimize the delay between in vivo and in vitro measurements. In this retrospective study, the first 7 patients provided 28 in vivo–in vitro pairs for comparison. The number of scans per treatment cycle is listed in Supplemental Table 1 (supplemental materials are available at <http://jnm.snmjournals.org>). Urine sample volumes (~ 8 mL) were determined by net weight. All activities were measured in a dose calibrator (Capintec 25R) in a low-background environment, with the same model vial (plastic Vacuette Tube, 9 mL; Greiner Bio-One GmbH) and positioning. The dose calibrator ^{177}Lu settings had been determined by a National Institute of Standards and Technology–traceable ^{177}Lu sample, and the estimated error was under 2%. SPECT/CT imaging parameters were the same as for the phantom study configured in low-energy mode for the low-energy peak (low-energy 113-keV triple-energy window), except that 3 bed positions gave eyes-to-thighs tomography and a duration of 12 s/frame was used. All radiotracer activities were decay-corrected to the start of the scan time. Patient information (decay-corrected injected activity and weight) was used to scale measurements of absolute

concentration (MBq/mL) as SUV (g/mL). The institutional review board approved this retrospective study, and the requirement to obtain informed consent was waived.

Three users analyzed SPECT/CT images for in vivo urinary bladder radiotracer uptake with quantitative software (Q.Metrix; GE Healthcare) using 3 different methods for selecting the VOI (Supplemental Fig. 1). In method A, a nuclear medicine physician delineated the uptake in the bladder by visual estimation of the margins in the nuclear image. In method B, a physicist set a threshold such that all voxels included within the urinary bladder had measured radiotracer concentrations greater than or equal to 42%, the maximum voxel value within the selected VOI (Fig. 1), consistent with methods for finding metabolic tumor volume in PET (28), and a reasonable threshold for SPECT volume quantitation under clinical acquisition conditions (29). In method C, a naïve user (a junior physicist) selected a sphere of maximal size that could fit within the urinary bladder as displayed in the CT images. The CT and SPECT images were coregistered, with the VOIs displayed on both. All users ensured that the VOIs fell within the anatomic region of the urinary bladder as found in the CT images. Partial-volume corrections were not a feature of the commercial quantitative software used, so a relatively large volume of expected homogeneous uptake (urinary bladder) was chosen for the validation. The quantitative software provided average radiotracer concentrations within the VOIs, scaled in units of absolute radiotracer concentration (MBq/mL) and SUV (g/mL).

Any in vivo–in vitro identity relations were determined by weighted linear regression (ideally slope = 1, intercept = 0) within a 95% confidence interval, with outliers identified and rejected for pairs exceeding a threshold of 3 times the mean Cook distance for the regression (30,31). Agreement between any 2 observers for the in vivo quantitation was measured by Cohen κ -statistics. The level of

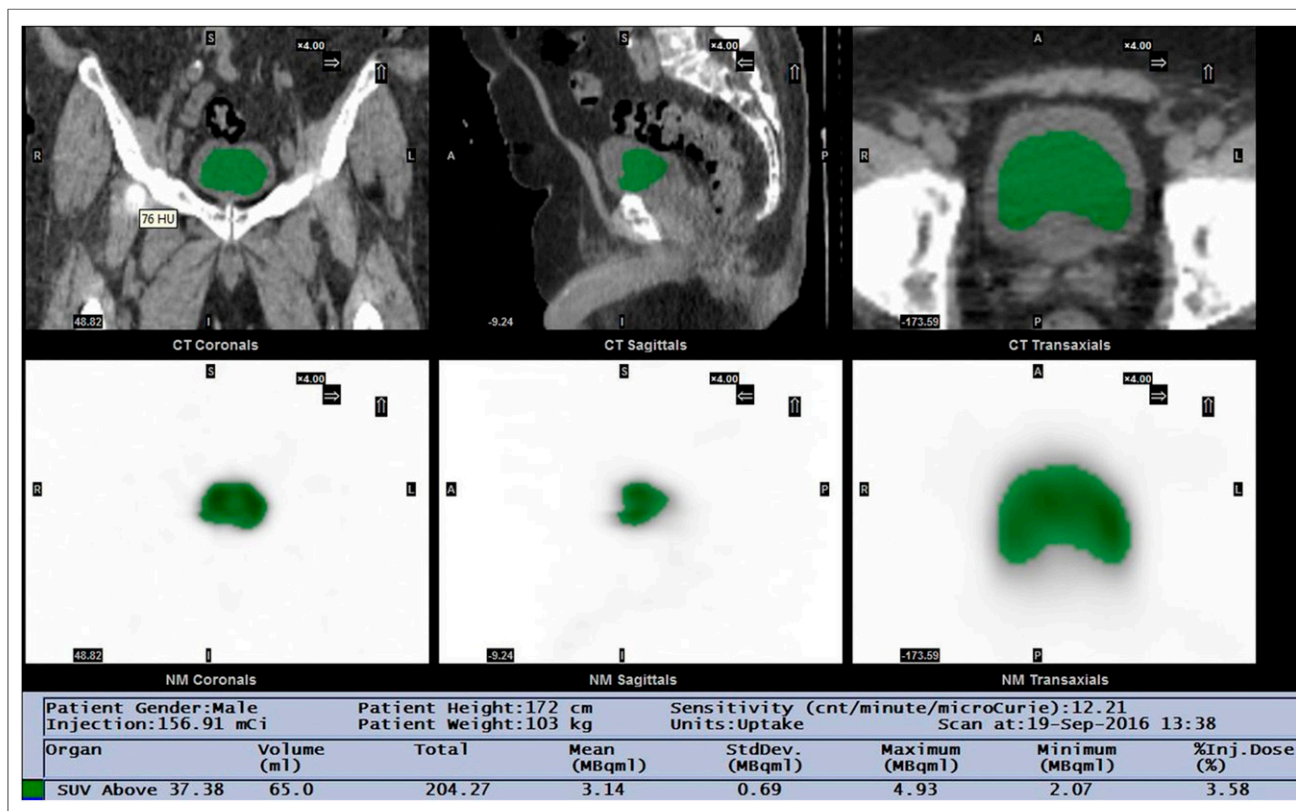


FIGURE 1. In vivo (SPECT) measurements. Example screenshot is shown of clinical quantitative software utility for method B. CT images (top) confirm that VOI selected (green) on SPECT images (bottom) falls within urinary bladder. Absolute quantitative measurements are shown in text at bottom.

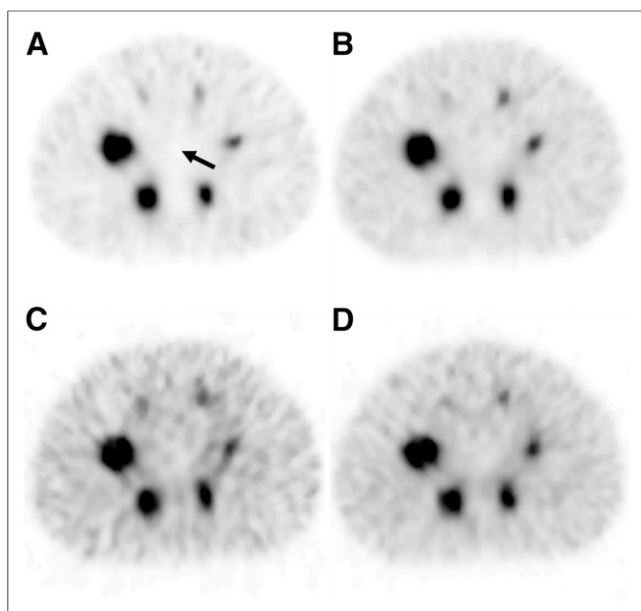


FIGURE 2. Transverse images of hot spheres for 4 phantom acquisition methods: low-energy 113-keV triple-energy window (A), high-energy 113- and 208-keV triple-energy window (B), high-energy 208-keV triple-energy window (C), and high-energy 208-keV dual-energy window (D). Imaging with lower energy peak only (A) minimized residual error in cold lung insert (arrow) compared with other acquisitions, which used high-energy peak.

agreement as per the κ -results were interpreted as poor ($\kappa \leq 0.20$), fair, ($0.20 < \kappa \leq 0.40$), moderate ($0.40 < \kappa \leq 0.60$), good ($0.60 < \kappa \leq 0.80$), very good ($0.80 < \kappa \leq 0.90$), or excellent ($\kappa > 0.90$), with a statistical significance level of less than 0.05.

RESULTS

Phantom Study

Phantom SPECT imaging established the camera volume sensitivities to be 5.5, 10.8, 6.1, and 6.7 $\text{s}^{-1} \text{MBq}^{-1}$ for acquisition methods low-energy 113-keV triple-energy window, high-energy 113- and 208-keV triple-energy window, high-energy 208-keV

TABLE 3
Comparison of Methods for Phantom Acquisition

Method	Background error (%)	Lung residual error (%)	Recovery coefficient MSE
LE 113 TEW	-5.0 ± 3.0	58.5 ± 9.7	0.26 ± 0.24
HE 113, 208 TEW	-8.6 ± 2.9	67.9 ± 5.1	0.35 ± 0.25
HE 208 TEW	-4.5 ± 2.1	68.4 ± 6.3	0.35 ± 0.20
HE 208 DEW	-8.3 ± 2.7	70.0 ± 7.5	0.43 ± 0.20

MSE = mean squared error; LE and HE = low and high energy, respectively; 113 and 208 = 113 and 208 keV, respectively; TEW and DEW = triple- and dual-energy windows, respectively.

Data are mean \pm SD.

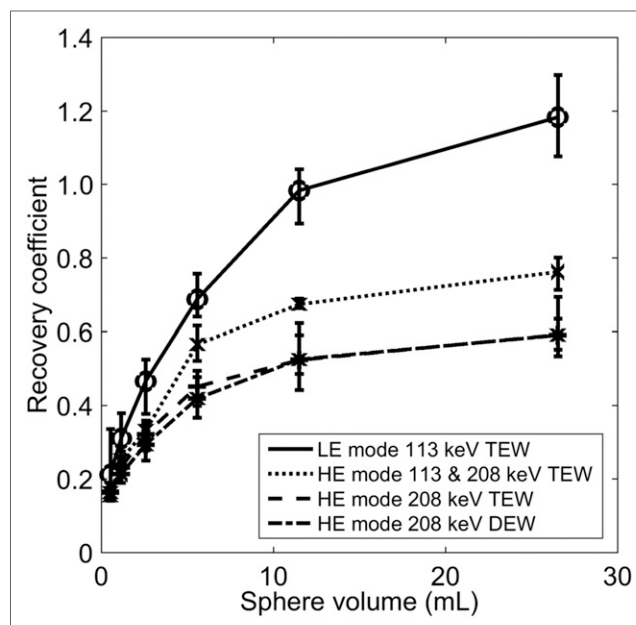


FIGURE 3. Recovery coefficients for SUV_{peak} of 4 phantom acquisition methods as per sphere volume. Imaging with lower energy peak provides better quantitation than including upper energy peak for this configuration of digital camera. DEW = dual-energy window; HE = high energy; LE = low energy; TEW = triple-energy window.

triple-energy window, and high-energy 208-keV dual-energy window, respectively. These sensitivity values were all within 13% of the planar sensitivities (6.2, 12.5, 6.1, and 6.0 $\text{s}^{-1} \text{MBq}^{-1}$, respectively). Imaging with the lower energy peak only (low-energy 113-keV triple-energy window) visibly minimized the artifactual uptake in the cold lung insert compared with the other acquisitions methods (Fig. 2). Adjusting window levels on the display made septal penetration clearly evident as streaking in the images incorporating the 208-keV peak. Table 3 shows that the lung residual error and the recovery coefficient mean squared error were significantly lower ($P < 0.05$) for low-energy 113-keV triple-energy window than for the other acquisition methods. Although the background error for low-energy 113-keV triple-energy window (-5%) was significantly lower than that for high-energy 208-keV triple-energy window and high-energy 208-keV dual-energy window, it did not significantly differ from high-energy 113- and 208-keV triple-energy window. A plot of recovery coefficients (Fig. 3) shows that for all hot sphere sizes, low-energy 113-keV triple-energy window gave values closer to unity than the other methods.

Clinical In Vivo-In Vitro Study

^{177}Lu -PSMA treatment doses ranged from 3.9 to 6.7 GBq (Supplemental Table 2). Urinary bladder sample concentrations ranged from 0.1 to 6.8 MBq/mL (Table 4), which, scaled for patient weight and activity at scan time, corresponded to SUVs ranging from 1.6 to 84 g/mL. Twenty-four in vivo-in vitro pairs were available for further analysis (Fig. 4), with 4 having been rejected as outliers via Cook distance calculations for the vivo-in vitro linear regression (30,31). All weighted linear regressions ($R^2 \geq 0.82$, $P < 0.0001$) provided identity in vivo-in vitro relations (confidence interval), with SUV averages from all users giving a slope of 0.96 ± 0.13 , an intercept of $-0.07 \pm 0.46 \text{ g/mL}$ (Table 5), and an average residual difference of 19.5%. The identity relation also held true when

TABLE 4
Radiotracer Concentrations In Vitro and In Vivo (Urine Sample/SPECT)

Study number	In vitro sample (MBq/mL)	In vivo method A (MBq/mL)	In vivo method B (MBq/mL)	In vivo method C (MBq/mL)
1	6.81	6.43 ± 2.12	7.68 ± 1.70	8.08 ± 1.72
2	0.31	0.31 ± 0.05	0.28 ± 0.05	0.28 ± 0.06
3	0.17	0.17 ± 0.04	0.18 ± 0.03	0.16 ± 0.04
4	0.13	0.11 ± 0.03	0.14 ± 0.02	0.09 ± 0.03
5	0.34	0.33 ± 0.04	0.26 ± 0.06	0.23 ± 0.09
6	0.16	0.16 ± 0.03	0.18 ± 0.02	0.16 ± 0.03
7	0.67	0.76 ± 0.09	0.70 ± 0.13	0.74 ± 0.12
8	0.78	0.78 ± 0.16	0.77 ± 0.17	0.77 ± 0.22
9	0.31	0.26 ± 0.04	0.22 ± 0.05	0.22 ± 0.07
10	2.99	3.04 ± 0.73	3.14 ± 0.69	3.15 ± 0.81
11	0.75	0.79 ± 0.16	0.82 ± 0.16	0.75 ± 0.22
12	0.10	0.14 ± 0.03	0.16 ± 0.03	0.12 ± 0.05
13	2.00	2.60 ± 0.64	2.77 ± 0.55	2.67 ± 0.73
14	0.71	0.69 ± 0.17	0.77 ± 0.15	0.50 ± 0.27
15	0.14	0.16 ± 0.05	0.22 ± 0.04	0.14 ± 0.07
16	1.93	3.06 ± 1.22	4.03 ± 0.86	2.98 ± 1.57
17	6.47	4.68 ± 0.34	3.59 ± 0.82	3.99 ± 0.75
18	1.25	1.02 ± 0.26	1.10 ± 0.24	0.96 ± 0.37
19	0.46	0.40 ± 0.05	0.33 ± 0.07	0.34 ± 0.10
20	4.57	3.14 ± 0.24	2.69 ± 0.52	3.00 ± 0.38
21	0.91	0.88 ± 0.13	0.74 ± 0.16	0.75 ± 0.24
22	0.11	0.11 ± 0.03	0.11 ± 0.03	0.10 ± 0.04
23	3.25	3.31 ± 0.56	2.73 ± 0.89	3.43 ± 0.46
24	0.24	0.24 ± 0.04	0.21 ± 0.04	0.17 ± 0.05
25	0.17	0.13 ± 0.02	0.12 ± 0.02	0.09 ± 0.03
26	1.56	1.66 ± 0.21	1.60 ± 0.26	1.62 ± 0.26
27	0.12	0.22 ± 0.05	0.26 ± 0.04	0.21 ± 0.06
28	1.19	1.35 ± 0.66	1.91 ± 0.41	1.35 ± 0.71

In vitro data are estimated at <2% uncertainty for in vitro samples. In vivo data are mean ± SD.

concentrations were scaled as MBq/mL (Table 5). Compared with the other 2 methods, method A (visual delineation VOI) provided the R^2 value closest to 1 and the lowest average residual difference in SUV: 15.4% compared with 24.2% and 22.0% for methods B (42% threshold VOI) and C (spheric VOI), respectively. The κ -agreement among the 3 methods of obtaining in vivo SUV was generally very good, ranging from 0.85 (0.79–0.91, confidence interval) between methods B and C to 0.87 (0.84–0.91, confidence interval) between methods A and C.

DISCUSSION

For phantom acquisitions, the best quantitative results with the CZT digital camera were from imaging the lower 113-keV peak of ^{177}Lu only, neglecting the higher 208-keV peak, but is likely not optimal. Collimator septal penetration was evident by the spillover of counts into the cold lung insert, reducing its contrast, and by the suppression of recovery coefficient values due to higher background counts when using the digital camera in high-energy mode.

This result contrasts with previous results for a standard γ -camera, in which a combination of data from the 2 energy peaks provided the best quantitation. However, in the previous study an effective source scatter estimation model was used and a medium-energy collimator was used (19). The latter difference reduces the septal penetration that was visually evident in the 3 acquisition high-energy modes of the CZT camera. When medium-energy collimation becomes readily available for the digital camera, the inclusion of the higher-energy peak in ^{177}Lu image quantitation should be revisited and will likely be the preferred methodology.

The sensitivity of this γ -camera configuration for the 113-keV ($6.2 \text{ s}^{-1} \text{ MBq}^{-1}$) and 208-keV ($6.1 \text{ s}^{-1} \text{ MBq}^{-1}$) emissions were similar to each other and similar to a commercial sodium iodide γ -camera with a 1-cm-thick crystal and medium-energy collimation (4). The lower photopeak detection efficiencies at the higher energy are compensated by the higher γ -ray emission intensity (Table 1). More current models of this camera use collimators with 4.5-mm hole lengths and CZT crystals 7.25 mm in thickness, instead of 5 mm. Consequently, the camera sensitivities for ^{177}Lu

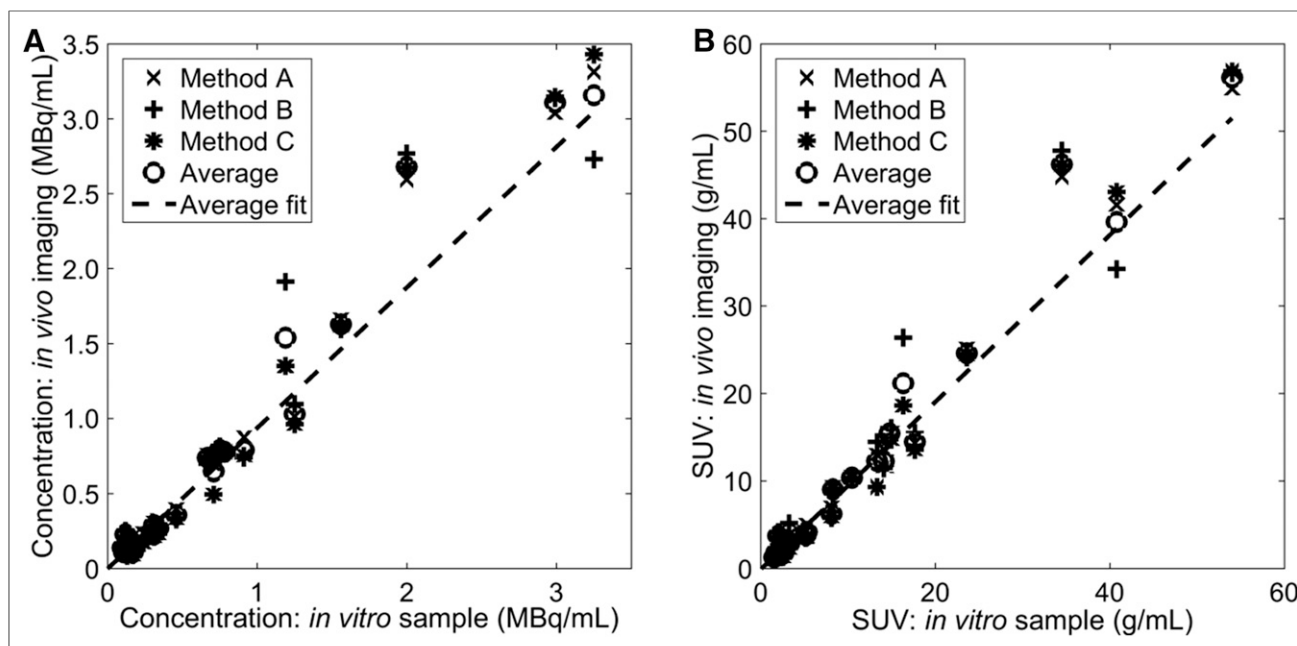


FIGURE 4. In vivo SPECT vs. in vitro urinary sample measurements: concentration (A) and SUV_{peak} (B).

are expected to be somewhat improved over the values reported here, as has been found for ^{99m}Tc sensitivity values (21).

For CZT detectors, energy windows set below the photopeak can be expected to include events from the photopeak itself because of incomplete charge collection and incomplete photon detection (32). Consequently, the scatter component is overestimated in the forward projector during image reconstruction, diminishing the relative contribution of the photopeak component. The SPECT calibration from the phantom study ameliorates this effect somewhat, but this is a suboptimal solution and relies on phantom and patient geometries being similar with respect to scatter. The average quantitation error of 20% reported here could likely be improved by

reducing scatter correction errors. Modeling and deconvolution (32) methods have been implemented to improve scatter correction in CZT dedicated cardiac SPECT cameras but are not part of the vendor-supplied quantitative software used in this study.

For the patient study, there was an identity relationship between in vitro and in vivo measurements of urinary-bladder-sampling radiotracer concentrations scaled as volumetric activity (MBq/mL) or as SUV (g/mL). Regardless of the collimator septal penetration by higher-energy photons, acquisitions with the 113-keV peak energy window provided reasonable quantitative SPECT results with this digital camera configuration. All methods gave an identity relationship, although method A, visual assessment of the VOI, had

TABLE 5
Linear Regression Parameters for In Vivo SPECT vs. In Vitro Sample Measurements

Parameter	Method			Average
	A	B	C	
SUV				
Slope	0.996	0.926	0.985	0.956
95% CI slope	0.893→1.10	0.732→1.113	0.856→1.115	0.823→1.088
Intercept (g/mL)	-0.157	0.239	-0.351	-0.070
95% CI intercept	-0.550→0.235	-0.353→0.841	-0.815→0.113	-0.531→0.390
R^2	0.948	0.829	0.919	0.910
Concentration				
Slope	0.9835	0.887	0.977	0.938
95% CI slope	0.880→1.09	0.705→1.068	0.840→1.108	0.800→1.076
Intercept (MBq/mL)	-0.006	0.026	-0.022	0.000
95% CI intercept	-0.032→0.020	-0.013→0.656	-0.055→0.011	-0.032→0.033
R^2	0.946	0.824	0.916	0.900

CI = confidence interval.

the best fit to the line of identity to the extent that it provided for the slope closest to 1, the intercept closest to 0, the R^2 value closest to 1, and the lowest average residual errors. Although this finding suggests good accuracy for a trained eye using the digital SPECT and the quantitative software, this method is the most subjective and presents challenges to routine use. In general, there was very good agreement among the 3 users applying the different methods of in vivo measurement ($\kappa > 0.8$). Considering that routine ^{177}Lu dosimetry presents a nonnegligible workload, much of which likely needs to be performed by technicians (23), proper staff training is probably the key to the use of quantitative SPECT results in dosimetry.

CONCLUSION

Quantitative results for SPECT ^{177}Lu imaging were optimal for the low-energy mode of the CZT digital camera with wide-energy high-resolution collimation. Urinary bladder concentrations of the theranostic radiopharmaceutical, ^{177}Lu -PSMA, can be measured in vivo using a solid-state SPECT/CT camera and a clinical quantitative software package, to within a good proximity of in vitro results. This practical, noninvasive, in vivo quantitation method can potentially improve diagnosis, improve treatment tailoring and response assessment, and provide data essential to dosimetry.

DISCLOSURE

No potential conflict of interest relevant to this article was reported.

KEY POINTS

QUESTION: How accurate is in vivo quantitation of ^{177}Lu radiotracer concentration using a digital solid-state SPECT system compared with gold standard in vitro measurements?

PERTINENT FINDINGS: In vivo quantitation of ^{177}Lu radiotracer concentration in a digital solid-state SPECT system agrees with in vitro urine sampling measurements to within about 20%.

IMPLICATIONS FOR PATIENT CARE: This practical, noninvasive, in vivo quantitation method can potentially improve diagnosis, improve treatment tailoring and response assessment, and provide data essential to dosimetry.

REFERENCES

- Kratochwil C, Giesel FL, Stefanova M, et al. PSMA-targeted radionuclide therapy of metastatic castration-resistant prostate cancer with ^{177}Lu -labeled PSMA-617. *J Nucl Med*. 2016;57:1170–1176.
- Langbein T, Weber WA, Eiber M. Future of theranostics: an outlook on precision oncology in nuclear medicine. *J Nucl Med*. 2019;60(suppl):13S–19S.
- Kratochwil C, Fendler WP, Eiber M, et al. EANM procedure guidelines for radionuclide therapy with ^{177}Lu -labelled PSMA-ligands (^{177}Lu -PSMA-RLT). *Eur J Nucl Med Mol Imaging*. 2019.
- Ljungberg M, Celler A, Konijnenberg MW, Eckerman KF, Dewaraja YK, Sjögren-Gleisner K. MIRD pamphlet no. 26: joint EANM/MIRD guidelines for quantitative ^{177}Lu SPECT applied for dosimetry of radiopharmaceutical therapy. *J Nucl Med*. 2016;57:151–162.
- Yordanova A, Becker A, Eppard E, et al. The impact of repeated cycles of radioligand therapy using [^{177}Lu] Lu-PSMA-617 on renal function in patients with hormone refractory metastatic prostate cancer. *Eur J Nucl Med Mol Imaging*. 2017;44:1473–1479.
- Sandström M, Garske U, Granberg D, Sundin A, Lundqvist H. Individualized dosimetry in patients undergoing therapy with ^{177}Lu -DOTA-D-Phe1-Tyr3-octreotate. *Eur J Nucl Med Mol Imaging*. 2010;37:212–225.
- Bodei L, Mueller-Brand J, Baum RP, et al. The joint IAEA, EANM, and SNMMI practical guidance on peptide receptor radionuclide therapy (PRRT) in neuroendocrine tumours. *Eur J Nucl Med Mol Imaging*. 2013;40:800–816.
- Hagmarker L, Svensson J, Ryden T, et al. Bone marrow absorbed doses and correlations with hematological response during ^{177}Lu -DOTATATE treatments are influenced by image-based dosimetry method and presence of skeletal metastases. *J Nucl Med*. 2019;60:1406–1413.
- Kafrouni M, Allimant C, Fourcade M, et al. Analysis of differences between $^{99\text{m}}\text{Tc}$ -MAA SPECT- and $^{90\text{Y}}$ -microsphere PET-based dosimetry for hepatocellular carcinoma selective internal radiation therapy. *EJNMMI Res*. 2019;9:62.
- Bailey DL, Willowson KP. An evidence-based review of quantitative SPECT imaging and potential clinical applications. *J Nucl Med*. 2013;54:83–89.
- King MA, Coleman M, Penney BC, Glick SJ. Activity quantitation in SPECT: a study of prereconstruction Metz filtering and the use of the scatter degradation factor. *Med Phys*. 1991;18:184–189.
- Walrand SHM, van Elmbt LR, Pauwels S. Quantitation in SPECT using an effective model of the scattering. *Phys Med Biol*. 1994;39:719–734.
- Fleming JS. A technique for using CT images in attenuation correction and quantification in SPECT. *Nucl Med Commun*. 1989;10:83–97.
- LaCroix KJ, Tsui BMW, Hasegawa BH, Brown JK. Investigation of the use of x-ray CT images for attenuation compensation in SPECT. *IEEE Trans Nucl Sci*. 1994;41:2793–2799.
- Bockisch A, Freudenberger LS, Schmidt D, Kuwert T. Hybrid imaging by SPECT/CT and PET/CT: proven outcomes in cancer imaging. *Semin Nucl Med*. 2009;39:276–289.
- Na CJ, Kim J, Choi S, et al. The clinical value of hybrid sentinel lymphoscintigraphy to predict metastatic sentinel lymph nodes in breast cancer. *Nucl Med Mol Imaging*. 2015;49:26–32.
- Suh M, Cheon GJ, Seo HJ, Kim HH, Lee DS. Usefulness of additional SPECT/CT identifying lymphatico-renal shunt in a patient with chyluria. *Nucl Med Mol Imaging*. 2015;49:61–64.
- Kennedy JA, Reizberg I, Lugassi R, Himmelman S, Keidar Z. Absolute radio-tracer concentration measurement using whole-body solid-state SPECT/CT technology: in vivo/in vitro validation. *Med Biol Eng Comput*. 2019;57:1581–1590.
- de Nijs R, Lagerburg V, Klausena TL, Holma S. Improving quantitative dosimetry in ^{177}Lu -DOTATATE SPECT by energy window-based scatter corrections. *Nucl Med Commun*. 2014;35:522–533.
- Bailey DL, Hennessy TM, Willowson KP, et al. In vivo quantification of ^{177}Lu with planar whole-body and SPECT/CT gamma camera imaging. *EJNMMI Phys*. 2015;2:20.
- Kennedy JA, Lugassi R, Keidar Z. Digital SPECT: collimator design and CZT crystal thickness affect general purpose solid state camera characteristics facilitating dual isotope $^{99\text{m}}\text{Tc}/^{123}\text{I}$ quantitation [abstract]. *Eur J Nucl Med Mol Imaging*. 2019;46(suppl 1):S274.
- National Electrical Manufacturers Association. *Performance Measurements of Gamma Cameras*. Rosslyn, VA: National Electrical Manufacturers Association; 2012. NEMA standards publication NU 1-2012.
- Ljungberg M, Sjögren-Gleisner K. Three-dimensional image-based dosimetry in radionuclide therapy. *IEEE Trans Radiat Plasma Med Sci*. 2018;2:527–540.
- Delker A, Fendler WP, Kratochwil C, et al. Dosimetry for ^{177}Lu -DKFZ-PSMA-617: a new radiopharmaceutical for the treatment of metastatic prostate cancer. *Eur J Nucl Med Mol Imaging*. 2016;43:42–51.
- IAEA. *IAEA Human Health Series No. 1: Quality Assurance for PET and PET/CT Systems*. Vienna, Austria: International Atomic Energy Agency; 2009.
- Vanderhoeck M, Perlman SB, Jeraj R. Impact of the definition of peak standardized uptake value on quantification of treatment response. *J Nucl Med*. 2012;53:4–11.
- Zeintl J, Vija AH, Yahil A, Hornegger J, Kuwert T. Quantitative accuracy of clinical $^{99\text{m}}\text{Tc}$ SPECT/CT using ordered-subset expectation maximization with 3-dimensional resolution recovery, attenuation, and scatter correction. *J Nucl Med*. 2010;51:921–928.
- Hatt M, Le Rest CC, Albarghach N, Pradier O, Visvikis D. PET functional volume delineation: a robustness and repeatability study. *Eur J Nucl Med Mol Imaging*. 2011;38:663–672.
- King MA, Long DT, Brill AB. SPECT volume quantitation: influence of spatial resolution, source size and shape, and voxel size. *Med Phys*. 1991;18:1016–1024.
- Bollen KA, Jackman RW. Regression diagnostics: an expository treatment of outliers and influential cases. In: Fox J, Long JS, eds. *Modern Methods of Data Analysis*. Newbury Park, CA: Sage; 1990:257–291.
- MATLAB and Statistics Toolbox Release 2015b. Natick, MA: The MathWorks, Inc.; 2015.
- Kacperski K, Erlandsson K, Ben-Haim S, Hutton BF. Iterative deconvolution of simultaneous $^{99\text{m}}\text{Tc}$ and ^{201}Tl projection data measured on a CdZnTe-based cardiac SPECT scanner. *Phys Med Biol*. 2011;56:1397–1414.